Evaluation of the Spectral Fit Algorithm as Functions of Frequency Range and Δka_{eff}

Timothy A. Bigelow, *Member, IEEE*, and William D. O'Brien, Jr., *Fellow, IEEE*

***Abstract*—Considerable effort has been directed at quantifying the properties of the tissue microstructure (i.e., scatterer correlation length) to diagnose disease and monitor treatment. In vivo assessments have had limited success due to frequency-dependent attenuation along the propagation path (i.e., total attenuation) masking the frequency dependence of the scattering from the tissue microstructure. Previously, both total attenuation and scatterer correlation length, given by the effective radius, were solved simultaneously by a two-parameter minimization of the mean squared error between a reference spectrum, modified by the attenuation and scatterer effective radius, and the backscattered waveforms using an algorithm termed the spectral fit algorithm. Herein, the impact of frequency range (largest frequency minus smallest frequency) and Δka_{eff} (largest ka_{eff} value minus smallest ka_{eff} value; k is wave number and a_{eff} is scatterer effective radius) used by the spectral fit algorithm on estimating the scatterer effective radius, and total attenuation was assessed by computer simulations while excluding frequencies of the backscattered power spectrum dominated by electronic noise. The simulations varied the effective radius of the scatterers (5 μm to 150 μm), the attenuation of the region (0 to 1 dB/cm-MHz), the bandwidth of the source, and the amount of electronic noise added to the radio frequency (rf) waveforms. The center frequency of the source was maintained at 8 MHz. Comparable accuracy and precision of the scatterer effective radius were obtained for all the simulations whenever the same Δka_{eff} was used to obtain the estimates. A Δka_{eff} of 1 gave an accuracy and precision of $\sim$15% $\pm$ 35%, and a width of 1.5 gave an accuracy and precision of $\sim$5% $\pm$ 15% consistently for all of the simulations. Similarly, the accuracy and precision of the total attenuation estimate were improved by increasing the frequency range used by the spectral fit algorithm.**

I. Introduction

The use of medical ultrasound to quantify the tissue microstructure for the purpose of disease diagnosis and treatment assessment has been studied by different investigators for almost 30 years [1]–[6]. During that time, the quantification of the tissue microstructure has shown great potential. Lizzi *et al.* [7] were able to observe changes in the tissue microstructure that correlated with tissue necrosis in ultrasound therapy applications of tumors in the eye. Oelze *et al.* [6] showed that the tissue microstructure could distinguish between fibroadenomas and carcinomas. Likewise, Tateishi *et al.* [8] demonstrated that the tissue microstructure could be used to diagnose axillary lymph node metastases in breast cancer, and Feleppa *et al.* [9], [10] used tissue microstructure to identify cancer in the prostate. As well as these examples involving tumors, Insana *et al.* [11] used the properties of the tissue microstructure obtained from backscattered ultrasound signals to measure the structural properties of the kidney.

Despite the aforementioned successes, the quantification of the tissue microstructure using backscattered radio frequency (rf) waveforms has had only limited success in clinical applications due largely to the frequency-dependent attenuation along the propagation path masking the frequency dependence of the backscattered signals. The frequency dependence of the backscattered waveforms is needed to estimate the effective radius of the tissue microstructure, one of the most important diagnostic properties [4]. Unfortunately, the attenuation along the propagation path (i.e., total attenuation) is different for every patient and must be determined on a patient-specific basis if the full potential of quantitative ultrasound is to be realized.

In our previous work [12], a new algorithm was introduced that estimated both the effective radius of the tissue microstructure and the total attenuation simultaneously and was termed the spectral fit (SF) algorithm. The SF algorithm requires that the form factor for the scatterers and the frequency dependence of the total attenuation (i.e., often assumed linear) to be known. The total attenuation and scatterer effective radius then are determined by a single minimization routine that fits a curve to the backscattered power spectrum, assuming the scatterers satisfy the Born approximation. The fitting procedure is very similar to that described by Insana *et al.* [4] when the attenuation is known. However, two parameters (i.e., attenuation and scatterer effective radius) are estimated instead of only scatterer effective radius. Also, unlike the approach by He and Greenleaf [13] who used the entire backscattered rf echo to estimate the total attenuation for which tissue heterogeneities along the propagation path would introduce errors, only the echoes from the region of interest (ROI) were needed to obtain the estimates of scatterer effective radius and total attenuation. Hence, tissue heterogeneity along the propagation path does not affect the estimates. Initially, the SF algorithm was proposed and validated, assuming that the window length used to gate the rf echoes in the time domain is small compared to the depth of focus for the source (i.e., local plane wave approximation) and assuming that the attenuation in the focal region (i.e., local attenuation) does not significantly alter the spectrum over the length of the window [12]. It may be possible to implement the algorithm without these assumptions in the future.

Manuscript received August 10, 2004; accepted March 23, 2005.

The authors are with the Bioacoustics Research Laboratory, Department of Electrical and Computer Engineering, University of Illinois, Urbana, IL 61801 (e-mail: wdo@uiuc.edu).

Although accurate effective radius and attenuation estimates were obtained using the SF algorithm, the precision of the estimates needed to be improved. Hence, the results were limited to quantifying larger tissue structures rather than forming a quantitative ultrasound (QUS) image of the tissue. The formation of a robust QUS image could potentially allow for early detection and diagnosis of tumors or other diseased states in tissue as well as the detection and diagnosis of features within a tumor such as a necrotic core. Furthermore, the precision and accuracy of the SF algorithm were degraded as the attenuation along the propagation path and amount of additive noise were increased.

In order to improve the precision of the SF algorithm, many different signal processing strategies were developed and evaluated [14]. Unfortunately, the precision was not significantly improved by any of the signal processing strategies. However, while performing the analysis of the different signal processing strategies, it was noted that the precision of the size estimates from the SF algorithm was better for larger scatterer effective radii when the same frequencies were used to obtain the estimates. Therefore, the goal of the work reported herein is to investigate the impact the choice of ka_{eff} values has on the accuracy and precision of the SF algorithm. In particular, this paper focuses on the relationship between the accuracy and precision of the SF algorithm to the size of the frequency range (i.e., largest frequency minus smallest frequency) and Δka_{eff} (i.e., largest ka_{eff} value minus smallest ka_{eff} value) used by the estimation routine. The relationship between frequency range (i.e., Δka_{eff}) and the precision of the scatterer effective radius estimate and related backscatter parameters has already been extensively investigated when the attenuation is assumed known [15]–[18] and, along with the window length, found to have a dominate role in setting the precision of the estimation scheme. Hence, investigating the importance of frequency range and Δka_{eff} is a logical first step in quantifying the SF algorithm. The analysis is done using computer simulations of Gaussian scatterers (i.e., scatterers with Gaussian spatial autocorrelation functions), a type of form factor, but the SF algorithm could be implemented with scatterers with different form factors [19].

II. Overview of Simulation Analysis

A. Review of Spectral Fit Algorithm

Before beginning our analysis of the importance of the Δka_{eff} and frequency ranges, the basics of the SF algorithm is briefly reviewed. The expected backscattered voltage squared returned from a tissue region that contains randomly positioned weak scatterers when using a weakly focused source is approximately proportional to [19] (see Table I for notation):

$$E\left[\left|V_{\text{refl}}(f)\right|^2\right] \propto f^4 \left|V_{\text{inc}}(f)\right|^2 \left|H(f)\right|^4 e^{-4\alpha_o z_T f} F_\gamma\left(f, a_{\text{eff}}\right), \tag{1}$$

if we assume that the total attenuation has a linear dependence on frequency. Likewise, the backscattered voltage squared returned from a rigid plane placed at the focal plane (i.e., a calibrated reference) is proportional to [20]:

$$\left|V_{\text{plane}}(f)\right|^2 \propto \left|V_{\text{inc}}(f)\right|^2 \left|H(f)\right|^4. \tag{2}$$

Hence, the expected backscattered voltage from the tissue region is proportional to the product of f^4, the reference power spectrum, a total attenuation term, and an effective radius term (i.e., form factor).

In the SF algorithm, an estimate for the expected backscattered voltage spectrum, denoted P_{scat}, is obtained by averaging the spectra of a set of independent backscattered rf waveforms in the normal frequency domain over a specified frequency range in which each waveform corresponds to a unique realization of a random distribution of scatterers. The selection of the frequency range used by the SF algorithm in this study will be discussed in the next section. After obtaining P_{scat}, the total attenuation along the propagation path α as well as the scatterer effective radius a_{eff} are determined by finding the values of α_o and a_{eff} that minimize the average squared difference (ASD) given by:

$$\text{ASD} = \underset{f}{\text{mean}}\left[\left(X\left(f,\, a_{\text{eff}},\, \alpha_o\right) - \overline{X}\left(a_{\text{eff}},\, \alpha_o\right)\right)^2\right], \tag{3}$$

where:

$$X\left(f,\, a_{\text{eff}},\, \alpha_o\right) = \ln\left(\frac{P_{\text{scat}}(f)}{\max\limits_f\left(P_{\text{scat}}(f)\right)}\right) - \ln\left(\frac{P_{\text{ref}}(f) F_\gamma\left(f, a_{\text{eff}}\right) e^{-4\alpha_o f z_T}}{\max\limits_f\left(P_{\text{ref}}(f) F_\gamma\left(f, a_{\text{eff}}\right) e^{-4\alpha_o f z_T}\right)}\right), \tag{4}$$

$$\overline{X}\left(a_{\text{eff}},\, \alpha_o\right) = \underset{f}{\text{mean}}\left[X\left(f,\, a_{\text{eff}},\, \alpha_o\right)\right],$$

and P_{ref} is given by:

$$P_{\text{ref}}(f) = k_o^4 \left|V_{\text{plane}}(f)\right|^2. \tag{5}$$

For a Gaussian scatterer, the ASD surface described by (3) has only one minimum so a simple minimization routine in MATLAB (The MathWorks Inc., Natick, MA) was used [14]. Subtracting by the modified P_{ref} term in X removes the system dependence of the backscattered power spectra. Also, subtracting by $\overline{X}$ removes the effects of any multiplicative constants, allowing estimation of scatterer effective radius and total attenuation independent of the acoustic concentration.

B. Simulation Parameters

In order to evaluate the impact the ka_{eff} values have on the SF algorithm, many different sets of simulations were performed. In the simulations, a weakly focused $f/4$ transducer with a focal length of 5 cm was used to ensonify

TABLE I
LIST OF SYMBOLS.

a_{eff}	=	effective radius, or correlation length, of scatterer.
$a_{\text{eff}\,j}$	=	estimated effective radius of scatterer found from one set (i.e., 25 averaged RF echoes) of simulated backscatter waveforms.
$\overline{a}_{\text{eff}}$	=	mean value of estimated effective radius from all sets of backscattered waveforms (i.e., $\overline{a}_{\text{eff}} = \sum_{\forall j} a_{\text{eff}\,j} \Big/ \sum_{\forall j} j$).
ASD	=	average squared difference term minimized by spectral fit algorithm.
$E[]$	=	expected value with respect to scattering random process.
f	=	frequency.
f_R	=	the parameter used to set the location of the Rayleigh function along the frequency axis (i.e., $\lvert f\rvert \cdot \exp\left(-\left(\frac{f-f_R}{\sigma_R}\right)^2\right)$).
$F_\gamma(f, a_{\text{eff}})$	=	form factor related to the scatterer geometry and effective radius.
g_{win}	=	windowing function used to gate the time-domain waveforms.
$H(f)$	=	filtering characteristics of ultrasound source.
k	=	wave number in tissue.
L	=	length of the windowing function.
n	=	power law dependence of real attenuation (i.e., $\alpha = \alpha_o f^n$).
N_{Floor}	=	noise floor of system used when selecting usable frequencies.
P_{ref}	=	reference spectrum. (i.e., $P_{\text{ref}}(f) = k_o^4 \lvert V_{\text{inc}}(f)\rvert^2 \lvert H(f)\rvert^4$).
P_{scat}	=	$E\left[\lvert V_{\text{refl}}\rvert^2\right]$ estimated from set of waveforms.
SNR	=	signal-to-noise ratio.
t	=	time.
V_{inc}	=	voltage spectrum applied to ultrasound source.
v_{noise}	=	example noise signal voltage in time domain (i.e., no signal transmitted by source).
V_{plane}	=	backscattered voltage spectrum from rigid plane placed at the focal plane.
V_{refl}	=	backscattered voltage spectrum from tissue containing scatterers.
$v_{refl\,i}$	=	voltage of an rf echo in time domain.
$X, \overline{X}$	=	terms used in minimization scheme for spectral fit algorithm.
z_T	=	distance from aperture plane to focal plane of ultrasound source.
α	=	total attenuation coefficient for tissue between ultrasound source and the region containing the scatterers (i.e., $\alpha = \alpha_o z_T$).
α_o	=	slope of total attenuation coefficient versus frequency.
$\underline{(a_o z_T)_j}$	=	estimated attenuation along the propagation path for single data set.
$\overline{(\alpha_o z_T)}$	=	mean value for attenuation along the propagation path from all sets of backscattered waveforms (i.e., $\overline{(\alpha_o z_T)} = \sum_{\forall j} (\alpha_o z_T)_j \Big/ \sum_{\forall j} j$).
$\sigma_{a_{\text{lower}}}$	=	percent deviation in values of scatterer effective radius for sizes smaller than the mean size (i.e., $a_{\text{eff}\,j} < \overline{a}_{\text{eff}}$).
$\sigma_{a_{\text{upper}}}$	=	percent deviation in values of scatterer effective radius for sizes larger than the mean size (i.e., $a_{\text{eff}\,j} > \overline{a}_{\text{eff}}$).
$\sigma_{\alpha_{\text{lower}}}$	=	deviation in dB/MHz in values of attenuation for attenuations smaller than the mean attenuation (i.e., $(\alpha_o z_T)_j < \overline{(\alpha_o z_T)}$).
$\sigma_{\alpha_{\text{upper}}}$	=	deviation in dB/MHz in values of attenuation for attenuations greater than the mean attenuation (i.e., $(\alpha_o z_T)_j > \overline{(\alpha_o z_T)}$).
σ_R	=	the bandwidth term for Rayleigh function (i.e., $\lvert f\rvert \cdot \exp\left(-\left(\frac{f-f_R}{\sigma_R}\right)^2\right)$).

an infinite half-space with scatterers placed at a density of $35/\text{mm}^3$. The scatterers had Gaussian autocorrelation functions (i.e., $F_\gamma(f, a_{\text{eff}}) = \exp\left(-0.827\,(k a_{\text{eff}})^2\right)$). The source was excited by an impulse function (i.e., $V_{\text{inc}}(f) = 1$), and the filtering characteristics for the source (i.e., $H(f)$) were given by:

$$H(f) = \frac{\lvert f\rvert \cdot \exp\left(-\left(\frac{f-f_R}{\sigma_R}\right)^2\right)}{\max\limits_{\forall f}\left(f \cdot \exp\left(-\left(\frac{f-f_R}{\sigma_R}\right)^2\right)\right)}, \tag{6}$$

where f_R was 8 MHz for all of the simulations and σ_R was varied to change the bandwidth of the source. A sampling frequency of 53 MHz was used when "digitizing" each of the waveforms so that the waveforms were sufficiently oversampled to facilitate electronic noise compensation. Electronic noise reduces the usable frequency range and broadens the backscattered spectrum. The broadening of the spectrum by the noise was compensated as is discussed in [19].

When estimating scattering parameters from the backscattered power spectrum, signal values dominated by electronic system noise must be excluded from the estimation scheme. Typically, this involves excluding the fre-

$$N_{\text{Floor}} = \max\left(\left[-20 \text{ mean}\left(10\log\left(\frac{P_{\text{scat}}\left(f_{N-200} : f_N\right)}{\max\limits_{\forall f}\left(\{P_{\text{scat}}(f)\}\,\text{Gaussian fit}\right)}\right)\right) + 6\right]\right). \tag{7}$$

quency components dominated by electronic noise, and only using a frequency range for which the values of the power spectrum correspond to tissue scattering. In the SF algorithm, the frequency range used to obtain the estimates was given by the range of frequencies corresponding to signal levels greater than the system noise floor (see (7) above). The −20 dB sets a limit on the frequency range in the absence of any electronic noise, and f_N refers to the largest positive frequency after taking the discrete Fourier transform of the sampled waveforms. Also, the signals were sufficiently oversampled so that at least the last 200 frequency samples would correspond to the additive white electronic system noise. Applying (7) automated the selection of the frequency range used by the SF algorithm and ensured that the estimates would not be corrupted by using spectral values dominated by noise. The size of the frequency range given by (7) is influenced by the bandwidth of the backscattered power spectrum in addition to the amount of electronic noise in the system.

For each of the simulated cases considered in this investigation, 1000 independent scatterer distributions were generated, and a waveform was calculated for each distribution as was done by Bigelow and O'Brien [20]. The resulting 1000 independent waveforms were combined into 40 sets with 25 waveforms per set yielding 40 estimates for each simulated case. The waveforms were windowed with a hamming window whose length varied from 1 to 8 mm and averaged in the normal spectral domain. The averaged spectrum then was compensated for windowing [19] and used in the SF algorithm to obtain an estimate for α and a_{eff}. The windowing compensation involves approximating the backscattered power spectrum and the Fourier transform of the windowing function as Gaussian functions. Then, the effect of windowing can be removed by multiplying the measured backscattered power spectrum by an appropriate Gaussian transformation.

III. Simulation Results

A. Source Bandwidths

The first simulations performed to assess the impact of using different $\Delta k a_{\text{eff}}$ and frequency ranges involved varying the bandwidth of the source and the effective radii of the Gaussian scatterers directly while maintaining the same value of half-space attenuation. The attenuation selected for the half-space was 0 dB/cm-MHz. However, the SF algorithm still solved for the attenuation as if it were unknown. Larger values of attenuation are considered in the next section. The bandwidth of the source was varied by changing the bandwidth of the Rayleigh function in (6) (i.e., σ_R) as 2, 4, and 6 MHz. The usable frequency range

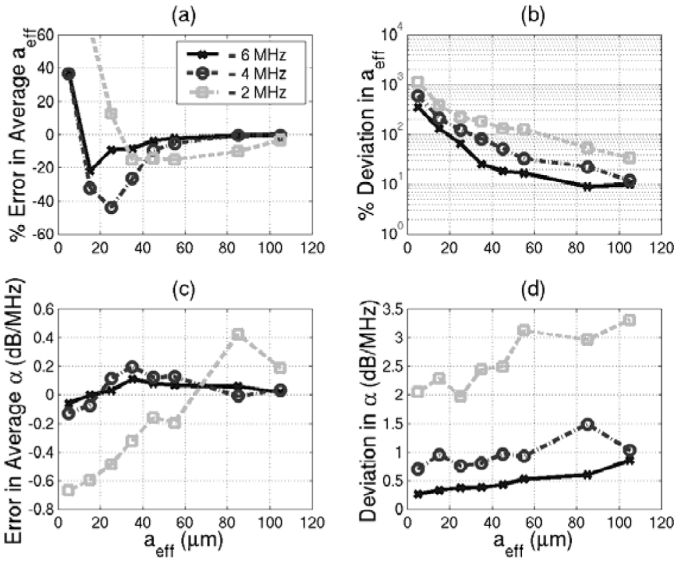

Fig. 1. Simulation results for different source bandwidths for (a) the percent error in the average scatterer size, (b) the percent deviation in the scatterer size, (c) the error in the average total attenuation, and (d) the deviation in the total attenuation as a function of scatterer size radii.

selected by (7) decreased as the bandwidth of the source decreased. For each source bandwidth, simulations were performed with scatterer effective radii varying from 5 to 65 μm in steps of 10 μm and from 65 to 105 μm in steps of 20 μm. Every scatterer had the same effective radius within each simulation.

The results at each bandwidth for a hamming window length of 3 mm for all of the scatterer effective radii are shown in Fig. 1. The results at a window length of 3 mm are representative of the other window lengths that are not shown which exhibited improved accuracy and precision with increasing window length. The average error was found by comparing the average value of all 40 estimates to the true value of scatterer effective radius and total attenuation. Likewise, the deviation was found by adding the standard deviations for estimates above and below the average value (i.e., $\sigma_{a_{\text{lower}}} + \sigma_{a_{\text{upper}}}$ and $\sigma_{\alpha_{\text{lower}}} + \sigma_{\alpha_{\text{upper}}}$) as given by:

$$\sigma_{a_{\text{upper}}} = \frac{100}{a_{\text{eff}}\Big|_{\text{Theory}}}\sqrt{\frac{\sum\limits_{\forall a_{\text{eff}\,j} > \overline{a}_{\text{eff}}}\left(a_{\text{eff}\,j} - \overline{a}_{\text{eff}}\right)^2}{\sum\limits_{\forall a_{\text{eff}\,j} > \overline{a}_{\text{eff}}} j}}$$

$$\sigma_{a_{\text{lower}}} = \frac{100}{a_{\text{eff}}\Big|_{\text{Theory}}}\sqrt{\frac{\sum\limits_{\forall a_{\text{eff}\,j} < \overline{a}_{\text{eff}}}\left(a_{\text{eff}\,j} - \overline{a}_{\text{eff}}\right)^2}{\sum\limits_{\forall a_{\text{eff}\,j} < \overline{a}_{\text{eff}}} j}}, \tag{8}$$

for the deviation in a_{eff} and:

$$\sigma_{\alpha_{\text{upper}}} = \sqrt{\frac{\sum_{\forall(\alpha_o z_T)_j > \overline{(\alpha_o z_T)}} \left((\alpha_o z_T)_j - \overline{(\alpha_o z_T)}\right)^2}{\sum_{\forall(\alpha_o z_T)_j > \overline{(\alpha_o z_T)}} j}}$$

$$\sigma_{\alpha_{\text{lower}}} = \sqrt{\frac{\sum_{\forall(\alpha_o z_T)_j < \overline{(\alpha_o z_T)}} \left((\alpha_o z_T)_j - \overline{(\alpha_o z_T)}\right)^2}{\sum_{\forall(\alpha_o z_T)_j < \overline{(\alpha_o z_T)}} j}}, \quad (9)$$

for the deviation in total attenuation [12]. These deviations above and below the mean were selected over the standard deviation for the analysis because the deviations above the mean were typically different from the deviations below the mean, especially for smaller, scatterer effective radii because the SF algorithm cannot yield a negative value for a_{eff}.

The precision of the scatterer effective radius estimates [Fig. 1(b)] significantly degraded with the smaller source bandwidths and smaller a_{eff} indicating a dependence on the range of ka_{eff} values used in the minimization routine. The precision was so poor (i.e., percent deviation greater than 200%) for scatterer effective radii less than ~35 μm for σ_R of 2 MHz, less than ~15 μm for σ_R of 4 MHz, and less than ~10 μm for σ_R of 6 MHz that the average error from the 40 estimates for each case [Fig. 1(a)] may not be an accurate measure of the accuracy of the SF algorithm. For larger values of scatterer effective radius for each value of σ_R, the accuracy of the scatterer size estimate also degrades with smaller source bandwidths and smaller a_{eff}, also indicating a dependence on Δka_{eff}. The dependence of the accuracy of the total attenuation estimate on the scatterer effective radius [Fig. 1(c)] is not conclusive. However, the precision [Fig. 1(d)] of the total attenuation estimates degrades slightly with increasing a_{eff}. Bigelow *et al.* [12] showed that increases in scatterer effective radius slightly reduce the usable frequency range obtained from (7) because the bandwidth of the backscattered power spectrum is reduced. Hence, the precision of the total attenuation estimate might depend on the frequency range used in the minimization routine and not depend on the scatterer effective radius directly.

In order to validate the dependence of the effective radius estimate on the range of ka_{eff} values and the dependence of the attenuation estimate on the range of frequencies, the results shown in Fig. 1 were replotted in Fig. 2 versus Δka_{eff} and frequency range for the effective radius and attenuation estimates, respectively. The accuracy [Fig. 2(a)] and precision [Fig. 2(b)] of the effective radius estimates exhibit a strong and consistent dependence on Δka_{eff} as is indicated by the overlapping curves. Hence, the scatterer effective radius estimate depends on Δka_{eff} and not just on the frequency range used to obtain the estimate. Likewise, precision [Fig. 2(d)] of the attenuation estimates exhibits a strong dependence on the frequency range used in (3). The dependence of the attenuation estimate on frequency range is not as consistent as the dependence of the effective radius estimate on Δka_{eff}, hence the attenuation estimate may be more strongly affected by other parameters of the estimation routine. Also, although accuracy of the attenuation estimate improves when using the σ_R of 6 MHz and σ_R of 4 MHz sources as compared to the σ_R of 2 MHz source [Fig. 2(c)], attributing the improvement to the increase in frequency range is not conclusive.

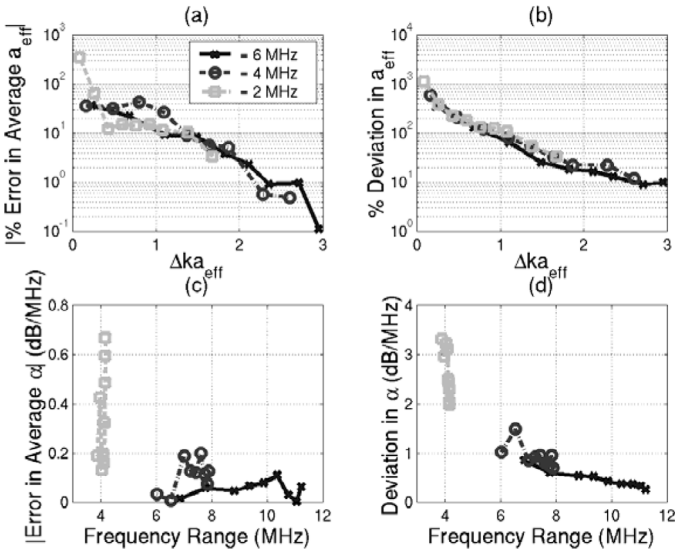

Fig. 2. Simulation results for different source bandwidths for (a) the percent error in the average scatterer size, (b) the percent deviation in the scatterer size, (c) the error in the average total attenuation, and (d) the deviation in the total attenuation as functions of Δka_{eff} and frequency range.

B. Total Attenuation

After showing that the accuracy and precision of the estimates were dependent on Δka_{eff} and the frequency range used when varying the bandwidth of the source, the attenuation of the half-space was varied to determine if associated changes in the Δka_{eff} and the frequency range also could explain the previously observed loss in precision with increasing attenuation [12]. The frequency range obtained from (7) would be decreased at larger half-space attenuation by the corresponding down shift of the spectrum. Hence, simulations were performed for half-space attenuation of 0.3, 0.5, and 1 dB/cm-MHz. For each value of half-space attenuation, the bandwidth of the source was held constant and set by using a σ_R value of 6 MHz in (6). For the 0.3 dB/cm-MHz half-space attenuation, the simulation was repeated for scatterer effective radii ranging from 5 to 75 μm in steps of 10 μm. Likewise, for the 0.5 and 1 dB/cm-MHz half-space attenuations, the scatterer effective radii ranged from 5 μm to 85 μm (steps of 10 μm) and 5 μm to 150 μm (steps of 10 to 20 μm), respectively. Simulations also were performed for a scatterer effective radius of 25 μm while varying the half-space attenuation from 0 to 1 dB/cm-MHz, similar to those previously per-

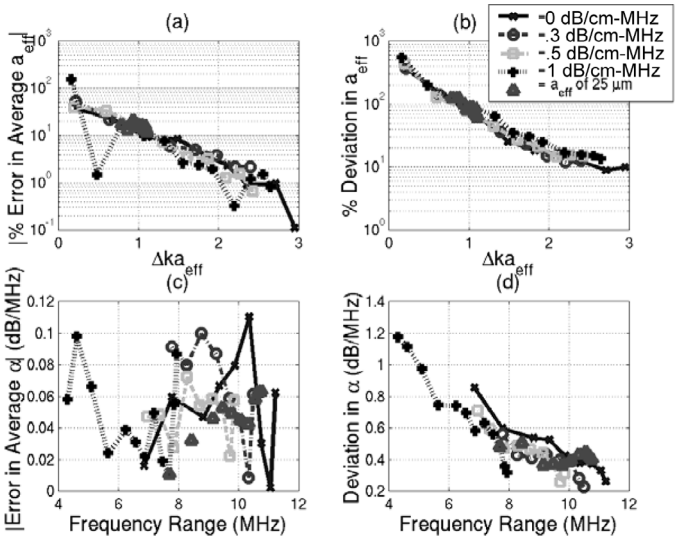

Fig. 3. Simulation results for different half-space attenuations for (a) the percent error in the average scatterer size, (b) the percent deviation in the scatterer size, (c) the error in the average total attenuation, and (d) the deviation in the total attenuation as functions of Δka_{eff} and frequency range.

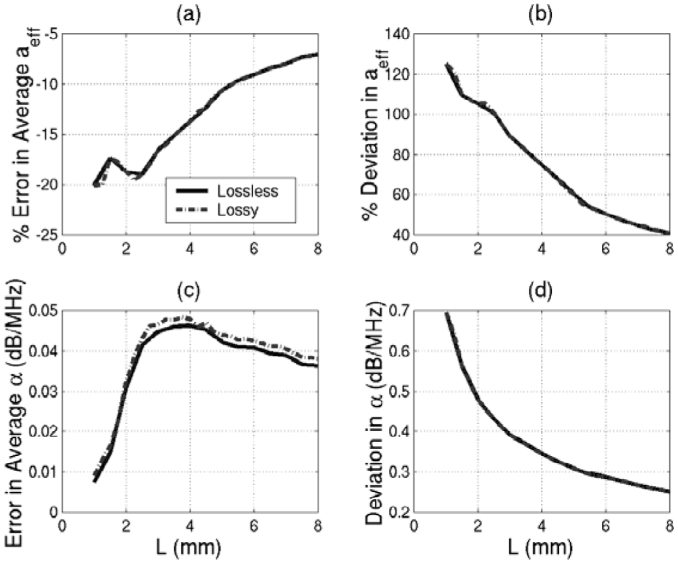

Fig. 4. Simulation results when the reference medium has an attenuation of 0.3 dB/cm-MHz (lossy) and 0 dB/cm-MHz (loss less) showing (a) the percent error in the average scatterer size, (b) the percent deviation in the scatterer size, (c) the error in the average total attenuation, and (d) the deviation in the total attenuation plotted versus window length for a half-space with an attenuation of 0.3 dB/cm-MHz containing 25-μm-radii scatterers.

formed [12]. Every scatterer had the same effective radius, and the attenuation of the half-space was homogeneous for any given simulation.

The results for the different scatterer effective radii and attenuations for a hamming window length of 3 mm are shown in Fig. 3. In addition to the four half-space attenuation cases just described, also included in the plot is the half-space attenuation of 0 dB/cm-MHz at a σ_R value of 6 MHz from Fig. 2. Once again, the accuracy [Fig. 3(a)] and precision [Fig. 3(b)] of the effective radius estimates exhibit a strong and consistent dependence on Δka_{eff} as is indicated by the overlapping curves. Likewise, the precision [Fig. 3(d)] of the total attenuation estimate seems to exhibit dependence on the frequency range used in (3). The dependence of the accuracy of the total attenuation estimate on the frequency range shown in Fig. 3(c) is once again not conclusive. Therefore, the degradation in the precision of the estimator observed by Bigelow *et al.* [19] for larger attenuations was due entirely to a smaller Δka_{eff} and a smaller frequency range. Hence, the amount of attenuation of the half-space, taken independently, relative to the attenuation of the medium used to acquire the reference spectrum (i.e., 0 dB/cm-MHz for water surrounding rigid plate) does not affect the performance of the SF algorithm.

To further demonstrate the lack of dependence of the algorithm on the attenuation of the half-space relative to the reference medium, a new reference waveform was acquired. This time, the attenuation of the medium between the source and reference plate placed at the focal plane was changed from 0 dB/cm-MHz (water) to 0.3 dB/cm-MHz. The new reference waveform then was used in the SF algorithm to estimate scatterer effective radius and total attenuation for a half-space with an attenuation of 0.3 dB/cm-MHz containing Gaussian scatterers with radii of 25 μm. The results for both the lossless (water) and lossy reference waveforms for this case are shown in Fig. 4. The results for the two different reference waveforms are identical, confirming that attenuation of the half-space relative to the reference does not matter provided that the same frequency range is used to obtain the estimates. This is in agreement with the work done by Huisman and Thijssen [17], who demonstrated that precision of their attenuation estimate was independent of the absolute attenuation and backscatter value.

C. Signal-to-Noise Ratio

In Bigelow *et al.* [19], the performance of the SF algorithm also was degraded by adding white "electronic" noise to the simulated waveforms. Hence, after completing the investigation on the impact of attenuation, the impact of adding white, Gaussian distributed noise to the acquired waveforms was investigated in greater detail in the present study. The waveforms selected for the investigation were for a half-space attenuation of 0 dB/cm-MHz, an σ_R of 6 MHz, and a scatterer effective radius of 105 μm. The amount of noise added to the waveforms was set by specifying the noise power relative to the signal backscattered from the reference plate placed at the focal plane in a water bath. The noise power was varied in a series of simulations so that the mean value of the signal-to-noise ratio (SNR), calculated according to Bigelow *et al.* [12]:

$$\text{SNR} = \frac{1}{25}\sum_{j=1}^{25}\left(10\cdot\log\left(\frac{\int\left(g_{\text{win}}(t)v_{refl_j}(t)\right)^2 dt}{\int\left(g_{\text{win}}(t)v_{\text{noise}}(t)\right)^2 dt}\right)\right), \quad (10)$$

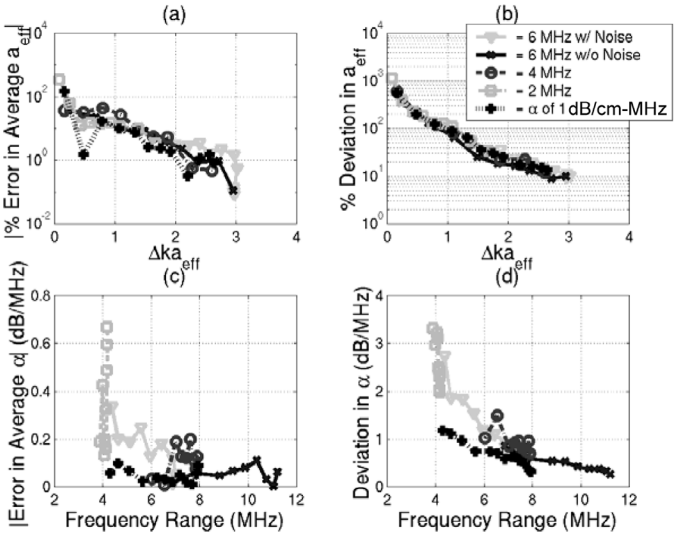

Fig. 5. Simulation results for different levels of electronic noise for (a) the percent error in the average scatterer size, (b) the percent deviation in the scatterer size, (c) the error in the average total attenuation, and (d) the deviation in the total attenuation plotted along with results for different bandwidth sources and a half-space attenuation of 1 dB/cm-MHz as functions of Δka_{eff} and frequency range.

for each of the 40 data sets (i.e., 1000 waveforms taken in sets of 25) varied from 36 to 3 dB. Because added electronic noise would increase N_{floor}, the usable frequency range selected by (7) was reduced by the addition of the noise.

The results for all of the different noise levels at a hamming window length of 3 mm are shown in Fig. 5. Also, the results without noise for σ_R values of 2 MHz, 4 MHz, and 6 MHz at an attenuation of 0 dB/cm-MHz from Fig. 2 and the results for an attenuation of 1 dB/cm-MHz from Fig. 3 are replotted in Fig. 5 for comparison. Once again, the accuracy and precision of the scatterer effective radius estimate for the noisy signals have the same dependence on Δka_{eff} that was observed in the earlier simulations [Figs. 5(a) and (b)]. Hence, the accuracy and precision of the scatterer effective radius estimate are a function of Δka_{eff} and not a function of SNR directly. The SNR only indirectly affects the accuracy/precision by reducing the usable frequency range (i.e., Δka_{eff}) obtained from (7).

Also, the precision of the total attenuation estimate appears to have the same dependence on the frequency range that was observed in the earlier simulations shown in Fig. 2 that varied the value of σ_R [Fig. 5(d)]. However, the precision of the attenuation estimate for the half-space attenuation of 1 dB/cm-MHz at smaller frequency ranges (i.e., less than 6 MHz) appears to be better than that expected by the other simulations. This difference was not noticed previously because of the gap in data for the frequency range from 4 to 6 MHz. From this we can conclude that, although the precision of the attenuation estimate is improved with increasing frequency range, the exact amount of improvement may be difficult to predict from the frequency range alone.

In the previous sections, the dependence of the accuracy of the attenuation estimate on frequency range was not conclusive. However, varying the SNR to change the frequency range [Fig. 5(c)] exhibits a clear improvement in the estimate with increasing frequency range. Also, the SNR results appear to bridge the gap between the results for the σ_R of 6 MHz and σ_R of 2 MHz sources, and the results for the half-space attenuation of 1 dB/cm-MHz give consistently more accurate estimates. Hence, the accuracy of the attenuation estimate, although dependent on the frequency range, also must have a strong dependence on other properties of the backscattered power spectrum.

IV. Discussion

In this paper, the impact of Δka_{eff} and the frequency range on the accuracy and precision of the SF algorithm were investigated. The accuracy and precision of the attenuation estimate were improved by increasing the frequency range, and the accuracy and precision of the scatterer effective radius estimate were consistently improved by increasing Δka_{eff}. The improvement explained the dependence of precision on half-space attenuation and electronic noise that was observed in Bigelow *et al.* [19]. Also, the effective radius and attenuation estimates were shown to be independent of the exact value of the total attenuation as also was demonstrated by Huisman and Thijssen [17]. Based on these results, the only definitive way to improve the robustness of the estimates of scatterer effective radius and total attenuation simultaneously is to use large frequency range and Δka_{eff}.

The importance of Δka_{eff} on the precision of the estimate of the effective radius may not be unique to the SF algorithm. Chaturvedi and Insana [18] performed a study in which they looked at the impact of frequency range on estimation precision when the attenuation was known for two different scatterer effective radii (100 μm and 150 μm). A comparison of precision results at the two radii reveals that the percent deviation is approximately the same for both radii for the same value of Δka_{eff}. Hence, the Δka_{eff} value also may set the precision of the traditional algorithm [4]. However, Chaturvedi and Insana's results [18] cannot be quantitatively compared to the results for the SF algorithm presented in this paper because the SF algorithm estimates both scatterer effective radius and total attenuation, and the traditional algorithm only estimates effective radius.

Before larger Δka_{eff} and frequency ranges can be used, several challenges remain to be addressed. First, in this paper, the attenuation always was assumed to have a strict linear dependence on frequency (i.e., $\alpha_o f$), although the scatterer size estimates would still be valid when the attenuation had a general linear dependence (i.e., $\alpha_o f + \alpha_b$). However, in real tissue, the attenuation has a power law dependence of the form $\alpha_o f^n$ [21]. Hence, a linear dependence ($\alpha_o f + \alpha_b$) is only valid over a limited frequency range. For larger frequency ranges, the linear approximation may need to be replaced with the complete power law dependence in the implementation of the SF algorithm in

which the best value of n for a class of QUS images would need to be experimentally determined.

Another challenge associated with larger frequency ranges is the presence of scatterers with different effective radii in the same tissue region. The current investigation only considered the estimation when a single effective radius was present. This was done because normally a single-effective radius in the tissue will be dominant over a certain range of frequencies. However, if the frequency range is increased, the effective radius estimate may be influenced by scattering structures on different size scales. It may be possible to construct form factors to deal with multiple effective radii in the same tissue region, allowing for the successful implementation of the SF algorithm. Also, after obtaining an accurate estimate for the total attenuation, the traditional algorithm could be implemented over a smaller portion of the frequency range to obtain estimates at the different size scales.

Acknowledgments

This work was supported by the University of Illinois Research Board, by a NDSEG Fellowship awarded to T. A. Bigelow, and by a Beckman Institute Graduate Fellowship awarded to T. A. Bigelow.

References

[1] R. C. Chivers and C. R. Hill, "A spectral approach to ultrasonic scattering from human tissue: Methods, objectives and backscattering measurements," *Phys. Med. Biol.*, vol. 20, no. 5, pp. 799–815, 1975.

[2] F. L. Lizzi, M. Greenebaum, E. J. Feleppa, and M. Elbaum, "Theoretical framework for spectrum analysis in ultrasonic tissue characterization," *J. Acoust. Soc. Amer.*, vol. 73, no. 4, pp. 1366–1373, 1983.

[3] D. K. Nassiri and C. R. Hill, "The use of angular acoustic scattering measurements to estimate structural parameters of human and animal tissues," *J. Acoust. Soc. Amer.*, vol. 79, no. 6, pp. 2048–2054, 1986.

[4] M. F. Insana, R. F. Wagner, D. G. Brown, and T. J. Hall, "Describing small-scale structure in random media using pulse-echo ultrasound," *J. Acoust. Soc. Amer.*, vol. 87, no. 1, pp. 179–192, 1990.

[5] T. J. Hall, M. F. Insana, L. A. Harrison, and G. G. Cox, "Ultrasonic measurement of glomerular diameters in normal adult humans," *Ultrasound Med. Biol.*, vol. 22, no. 8, pp. 987–997, 1996.

[6] M. L. Oelze, W. D. O'Brien, Jr., J. P. Blue, and J. F. Zachary, "Differentiation and characterization of rat mammary fibroadenomas and 4T1 mouse carcinomas using quantitative ultrasound imaging," *IEEE Trans. Med. Imag.*, vol. 23, no. 6, pp. 764–771, 2004.

[7] F. L. Lizzi, M. Astor, T. Liu, C. Deng, D. J. Coleman, and R. H. Silverman, "Ultrasonic spectrum analysis for tissue assays and therapy evaluation," *Int. J. Imaging Syst. Technol.*, vol. 8, pp. 3–10, 1997.

[8] T. Tateishi, J. Machi, E. J. Feleppa, R. Oishi, J. Jucha, E. Yanagihara, L. J. McCarthy, T. Noritomi, and K. Shirouzu, "In vitro diagnosis of axillary lymph node metastases in breast cancer by spectrum analysis of radio frequency echo signals," *Ultrasound Med. Biol.*, vol. 24, no. 8, pp. 1151–1159, 1998.

[9] E. J. Feleppa, A. Kalisz, J. B. Sokil-Melgar, F. L. Lizzi, T. Liu, A. Rosado, M. C. Shao, W. R. Fair, Y. Wang, M. S. Cookson, V. E. Reuter, and W. D. W. Heston, "Typing of prostate tissue by ultrasonic spectrum analysis," *IEEE Trans. Ultrason., Ferroelect., Freq. Contr.*, vol. 43, no. 4, pp. 609–619, 1996.

[10] E. J. Feleppa, T. Liu, A. Kalisz, M. C. Shao, N. Fleshner, V. Reuter, and W. R. Fair, "Ultrasonic spectral-parameter imaging of the prostate," *Int. J. Imaging Syst. Technol.*, vol. 8, no. 1, pp. 11–25, 1997.

[11] M. F. Insana, J. G. Wood, T. J. Hall, G. G. Cox, and L. A. Harrison, "Effects of endothelin-1 on renal microvasculature measured using quantitative ultrasound," *Ultrasound Med. Biol.*, vol. 21, no. 9, pp. 1143–1151, 1995.

[12] T. A. Bigelow, M. L. Oelze, and W. D. O'Brien, Jr., "Estimation of total attenuation and scatterer size from backscattered ultrasound waveforms," *J. Acoust. Soc. Amer.*, vol. 117, no. 3, pp. 1431–1439, 2005.

[13] P. He and J. F. Greenleaf, "Application of stochastic analysis to ultrasonic echoes—Estimation of attenuation and tissue heterogeneity from peaks of echo envelope," *J. Acoust. Soc. Amer.*, vol. 79, no. 2, pp. 526–534, 1986.

[14] T. A. Bigelow, "Estimating the medical ultrasound *in vivo* power spectrum," Ph.D. dissertation, University of Illinois at Urbana-Champaign, 2004.

[15] A. Gerig, J. Zagzebski, and T. Varghese, "Statistics of ultrasonic scatterer size estimation with a reference phantom," *J. Acoust. Soc. Amer.*, vol. 113, no. 6, pp. 3430–3437, 2003.

[16] F. L. Lizzi, E. J. Feleppa, M. Astor, and A. Kalisz, "Statistics of ultrasonic spectral parameters for prostate and liver examinations," *IEEE Trans. Ultrason., Ferroelect., Freq. Contr.*, vol. 44, no. 4, pp. 935–942, 1997.

[17] H. J. Huisman and J. M. Thijssen, "Precision and accuracy of acoustospectrographic parameters," *Ultrasound Med. Biol.*, vol. 22, no. 7, pp. 855–871, 1996.

[18] P. Chaturvedi and M. F. Insana, "Error bounds on ultrasonic scatterer size estimates," *J. Acoust. Soc. Amer.*, vol. 100, no. 1, pp. 392–399, 1996.

[19] T. A. Bigelow and W. D. O'Brien, Jr., "Signal processing strategies that improve performance and understanding of the quantitative ultrasound spectral fit algorithm," *J. Acoust. Soc. Amer.*, vol. 118, no. 3, pp. 1808–1819, 2005.

[20] T. A. Bigelow and W. D. O'Brien, Jr., "Scatterer size estimation in pulse-echo ultrasound using focused sources: Theoretical approximations and simulation analysis," *J. Acoust. Soc. Amer.*, vol. 116, no. 1, pp. 578–593, 2004.

[21] H. A. H. Jongen, J. M. Thijssen, M. Aarssen, and W. A. Verhoef, "A general model for the absorption of ultrasound by biological tissues and experimental verification," *J. Acoust. Soc. Amer.*, vol. 79, no. 2, pp. 535–540, 1986.

Timothy A. Bigelow was born in Colorado Springs, Colorado, on December 14, 1976. He graduated summa cum laude from Colorado State University in December 1998 with a B.S. degree in electrical engineering and a minor in mathematics. In August 1999, he began his graduate studies in electrical and computer engineering at the University of Illinois at Urbana-Champaign. During his graduate studies, he worked in the Bioacoustics Research Laboratory, where he completed his M.S. thesis on indicators of nonlinear propagation for focused ultrasound sources and his Ph.D. dissertation in April 2004 on ultrasound tissue characterization and attenuation estimation. While pursuing his graduate education, Dr. Bigelow was awarded a National Defense Science and Engineering Graduate Fellowship and a Beckman Institute Graduate Fellowship. Currently, Dr. Bigelow is a visiting assistant professor in the Electrical and Computer Engineering Department at the University of Illinois interested in ultrasound tissue characterization, ultrasound therapy, and ultrasound induced bioeffects.